NMDA receptor-dependent switching between different gamma rhythm-generating microcircuits in entorhinal cortex

Steven Middleton[a,1,2], Jozsi Jalics[b,1], Tilman Kispersky[c,1], Fiona E. N. LeBeau[a], Anita K. Roopun[a], Nancy J. Kopell[d,3], Miles A. Whittington[a], and Mark O. Cunningham[a,3]

[a]Institute of Neuroscience, Newcastle University, Newcastle NE2 4HH, United Kingdom; [b]Department of Mathematics and Statistics, Youngstown State University, One University Plaza, Youngstown, OH 44555; [c]Program in Neuroscience, Center for BioDynamics, Boston University, Boston, MA 02215; and [d]Department of Mathematics and Statistics, Center for BioDynamics, 111 Cummington Street, Boston University, Boston, MA 02215

Contributed by Nancy J. Kopell, September 25, 2008 (sent for review July 8, 2008)

Local circuits in the medial entorhinal cortex (mEC) and hippocampus generate gamma frequency population rhythms independently. Temporal interaction between these areas at gamma frequencies is implicated in memory—a phenomenon linked to activity of NMDA-subtype glutamate receptors. While blockade of NMDA receptors does not affect frequency of gamma rhythms in hippocampus, it exposes a second, lower frequency (25–35 Hz) gamma rhythm in mEC. In experiment and model, NMDA receptor-dependent mEC gamma rhythms were mediated by basket interneurons, but NMDA receptor-independent gamma rhythms were mediated by a novel interneuron subtype—the goblet cell. This cell was distinct from basket cells in morphology, intrinsic membrane properties and synaptic inputs. The two different gamma frequencies matched the different intrinsic frequencies in hippocampal areas CA3 and CA1, suggesting that NMDA receptor activation may control the nature of temporal interactions between mEC and hippocampus, thus influencing the pathway for information transfer between the two regions.

gamma oscillation | interneuron | ketamine

Gamma rhythms cover a broad range of frequencies from approximately 25 Hz up to, in some reports, over 100 Hz. Functional distinctions between different subbands of gamma rhythm are becoming apparent in neocortical studies (1). In the hippocampal–entorhinal axis a broad range of gamma frequencies has also been reported, with some suggestion, particularly from in vitro studies, of regional differences. For example, gamma rhythms generated in area CA3 in vitro and in vivo are generally in the 30–40 Hz range (2, 3), whereas gamma rhythms in area CA1 have been reported at higher frequencies (40–100 Hz) and were directly driven by entorhinal inputs (4). Any functional significance to these hippocampal frequency differences is not yet clear.

The basic mechanism of generation of population gamma rhythms by local neuronal circuits reveals an absolute dependence on the influence of fast spiking inhibitory interneurons at the level of principal cell somata (5, 6),with the frequency dependent on the magnitude and kinetics of gamma aminobutyric acid ($GABA_A$) receptor-mediated synaptic events (7). This mechanism can underlie gamma rhythms in a broad range of frequencies from around 20 Hz up to 70 Hz in the hippocampus (8) but cannot support higher frequencies such as those labeled as "high gamma" previously (9). This suggests that some semantic caution is required when ascribing mechanisms to rhythms labeled as "gamma" from in vivo studies. More than one subtype of fast-spiking interneuron has been shown to actively participate in gamma rhythms in the hippocampus (10–12). The latter study demonstrated gamma frequency outputs not only from perisomatic targeting basket cells (the accepted source of gamma frequency inhibitory inputs to principal cells (13), but also from trilaminar and bistratified interneurons with terminals predominantly in dendrite-containing laminae. This raises the possibility that different gamma rhythm generating local circuits, containing different interneuron subtypes, may coexist and be differentially activated under certain conditions (e.g., ref 14).

In the entorhinal cortex the predominant gamma frequency generating interneuron has been reported to be the superficial layer basket cell (15). This interneuron is highly sensitive to NMDA receptor-mediated excitation (16). However, blockade of NMDA receptor-mediated drive to superficial entorhinal cortex does not completely abolish gamma rhythms. The NMDA receptor antagonist ketamine leaves a residual gamma rhythm which is also dependent on $GABA_A$ receptor-mediated inhibition but does not require the NMDA-sensitive basket interneurons (17). These data suggest that different local circuit generators of gamma rhythms exist in the medial entorhinal cortex (mEC) that could be selectively activated on the basis of how much NMDA receptor activation incoming stimuli produce—a factor in neuronal communication long associated with memory formation (e.g., ref 18).

Given the importance of NMDA receptors in memory formation, and gamma rhythms in hippocampal-entorhinal communication associated with memory, we wished to study the effects of NMDA receptor activation on entorhinal rhythm generation in more detail. We use ketamine, which has been shown to affect memory processes along the hippocampal–entorhinal axis (19), to show that two interacting local circuits in medial entorhinal cortex exist, each capable of producing a gamma rhythm. These circuits consist of principal cell connections to two distinct subclasses of interneurons, one of which has not previously been characterized. Activation or blockade of NMDA receptors switches the relative dominance of the two interneurons in the local circuit, producing two gamma rhythms with distinct population frequencies and principal cell spike rates. The two gamma rhythms are ideally organized to communicate with the hippocampus through either the trisynaptic circuit—interacting with gamma rhythms in area CA3—or through a direct pathway—interacting with local circuit gamma rhythm generators in area CA1.

Results

Ketamine Changes Power and Frequency of Local Population Rhythms. Persistent gamma frequency oscillations were elicited in the superficial layers of mEC by bath application of kainate (mean frequency:

Author contributions: S.M., J.J., T.K., F.E.N.L., A.K.R., N.J.K., M.A.W., and M.O.C. designed research; S.M., J.J., T.K., F.E.L., A.K.R., M.A.W., and M.O.C. performed research; S.M., J.J., T.K., and N.J.K. analyzed data; and J.J., N.J.K., M.A.W., and M.O.C. wrote the paper.

The authors declare no conflict of interest.

See Commentary on page 18079.

[1]S.M., J.J., and T.K. contributed equally to this work.

[2]Present address: Laboratory for Neuronal Circuit Dynamics, RIKEN Brain Science Institute, 2-1 Hirosawa, Wako-shi, Saitama 351-0198, Japan.

[3]To whom correspondence may be addressed. E-mail: nk@math.bu.edu or mark.cunningham@ncl.ac.uk.

This article contains supporting information online at www.pnas.org/cgi/content/full/0809302105/DCSupplemental.

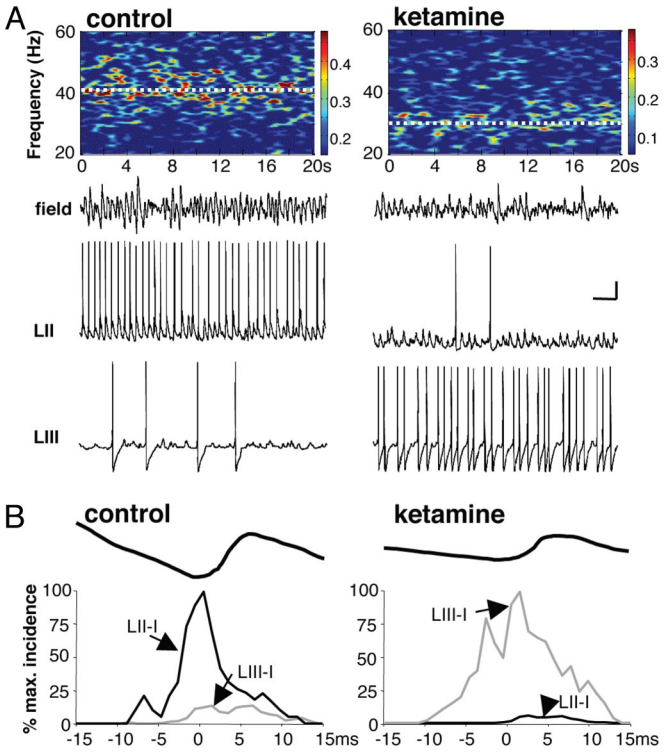

Fig. 1. NMDA receptor antagonism with ketamine reveals two local gamma rhythms mediated by different interneuron subtypes. (*A*) Example spectrograms from 20 s epoch of LII local field potential recording in the presence of kainate (400 nM), either without (control) or with ketamine (25 μM). Ketamine reduced gamma rhythm mean amplitude and frequency (41 Hz vs. 31 Hz). Example recordings show LII local field potential (field) and intracellular recordings from two types of interneuron, one with somata in LII (basket) and one with somata in LIII (goblet). Note the differential involvement of each interneuron subtype in the two conditions. (Scale bars, 0.1 mV (field), 10 mV (intracellular), 100 ms). (*B*) Relative spike rates and timings, relative to peak negativity in the field potential period. Example traces show roughly1 period (30 ms) mean band pass filtered (25–45 Hz) field potential centered around peak negativity used as the timing reference for concurrently recorded intracellular data. Graphs show global mean spike occurrences (n = 100 events from n = 5 cells of each type) quantified as probability of spike occurrence in each 1 ms bin per each gamma period, normalized to peak spike occurrence, in either cell, in each condition (control and in the presence of ketamine). Data from baskets (LII-I) is plotted in black, goblets (LIII-I) in gray.

41.2 ± 1.8Hz; mean power 2355 ± 189 μV (2), n = 6, Fig. 1*A*). In the presence of the NMDA receptor antagonist ketamine (25 μM), the peak frequency of population rhythm in superficial mEC was significantly reduced to 31 ± 3.2Hz ($P < 0.05$, n = 6, Fig. 1*A*). The power of population rhythm activity was also significantly reduced (468 ± 72μV (2); $P < 0.05$, n = 6). Previous studies (14) demonstrated that the gamma frequency field potential in mEC was generated predominantly by the phasic pattern of $GABA_A$ receptor-mediated inhibitory postsynaptic potentials (IPSPs) onto layer III pyramidal cells. Cross correlations between concurrently recorded field potentials and pyramidal cell IPSPs indicated a perisomatic origin of this phasic inhibition. We therefore tested whether the decrease in power and frequency of field potential gamma rhythms was accompanied by changes in the profile of IPSPs recorded in pyramidal cell somata. As with previous experiments (16), large amplitude IPSPs (9.2 ± 2.1 mV at −30 mV membrane potential) occurred at gamma frequencies (40 ± 4 Hz) in control conditions. In the presence of ketamine, somatic IPSP mean amplitude and frequency were significantly reduced in line with the changes in field potential (IPSP amplitude 4.8 ± 1.9 mV, frequency 28 ± 5 Hz, $P < 0.05$, n = 6, data not shown).

Different Interneuron Subtypes Are Involved in the Two Gamma Rhythms. The change in fast inhibitory inputs to pyramidal cells generated by ketamine can be explained by reduction in activity of fast-spiking, basket interneurons in superficial mEC. Both spike rates and membrane potential during gamma rhythms were significantly reduced by the NMDA receptor antagonist ketamine (Fig. 1*A*). In control gamma conditions, fast-spiking, basket-like mEC interneurons with cell bodies in LII (Fig. 1*A*) generated action potentials at a rate of 40 ± 2 Hz (n = 9), with action potentials phase locked to the peak negativity in the concurrently recorded field (Fig. 1*B*). Mean membrane potential of these interneurons during the gamma rhythm was −53 ± 4 mV. During the slower rhythm, in the presence of ketamine, spike rates in these interneurons were dramatically reduced. Spiking became more sporadic, with an overall, significantly lower mean rate of 3 ± 2Hz ($P < 0.05$, n = 9). Large amplitude, compound excitatory postsynaptic potentials were still evident (see below), but the reduced rate was accompanied by a significant reduction in mean membrane potential in the presence of ketamine (−58 ± 2 mV, $P < 0.05$, n = 9).

The decrease in basket interneuron excitability and subsequent spike rates appeared, superficially, to underlie the reduced power and frequency of the field potential gamma rhythm. However, the field gamma rhythm power fell to only about 20% of control values, pyramidal cell mean IPSP amplitude fell to only about 50%. In contrast, the output from basket cells fell to around 7% of control values. This almost complete abolition of basket cell-mediated inhibition in the network was at odds with the more subtle changes in the inhibition-based, field potential rhythm. These comparisons suggested involvement of other types of interneurons, not directly affected by NMDA receptor blockade, in the slower gamma rhythm seen in the presence of ketamine. One candidate interneuron subtype was found with cell bodies located in layer III. These interneurons were initially identified as having low spike rates during the control, field potential gamma rhythm. They had a goblet-like shape and generated outputs in bursts of 3–8 spikes with interspike intervals corresponding to theta frequencies (122 ± 17 ms). Overall mean spike rates were 3 ± 1 Hz (n = 7), with a mean resting membrane potential of −55 ± 1 mV (n = 7). In stark contrast to the behavior of basket cells on blockade of NMDA receptors, goblet interneurons significantly increased their firing rates. During the slower ketamine-induced gamma rhythm, firing rates increased significantly to 29 ± 5 Hz ($P < 0.05$, Fig. 1*A*), with spike incidence peaking just before or just after the peak negativity of the concurrently recorded field potential (Fig. *1B*). A depolarization in average membrane potential was seen in the presence of ketamine (−49 ± 2 mV, $P < 0.05$) indicating that goblet interneuron subtypes' responses to NMDA receptor blockade contrasted sharply with those of basket interneurons.

Neurolucida reconstruction of biocytin-filled basket and goblet interneurons showed differences in cytoarchitecture. Baskets had typical basket-like axonal arbors as previously described in mEC (16). Goblet interneurons had a characteristic "goblet-like" shape to their dendrites and axons. In the slice orientation used here, these goblet interneurons had two major dendritic processes extending laterally and up through the laminae toward the pial surface. They also possessed a short primary dendrite descending through LIII to lamina dissecans. Their axon arborized extensively and predominantly in LII with the lateral dendrites forming the boundary for horizontal axon arborization (Fig. 2). Despite their differing appearances, both interneuron subtypes responded in a similar, fast spiking manner to depolarizing current injection. However, input-output curves were considerably less linear for goblet cells [see supporting information (SI) Fig. S1] and spike shapes were also significantly different. Spike width at half height was 0.44 ± 0.03 ms and 0.69 ± 0.01 ms for basket and goblet cells, respectively ($P <$ 0.05, n = 5). The AHP of goblet cells (−16.3 ± 0.6 mV) was significantly larger than that observed in the basket cells (−13.5 ± 0.4 mV)($P < 0.05$, n = 5). In addition, the time from action

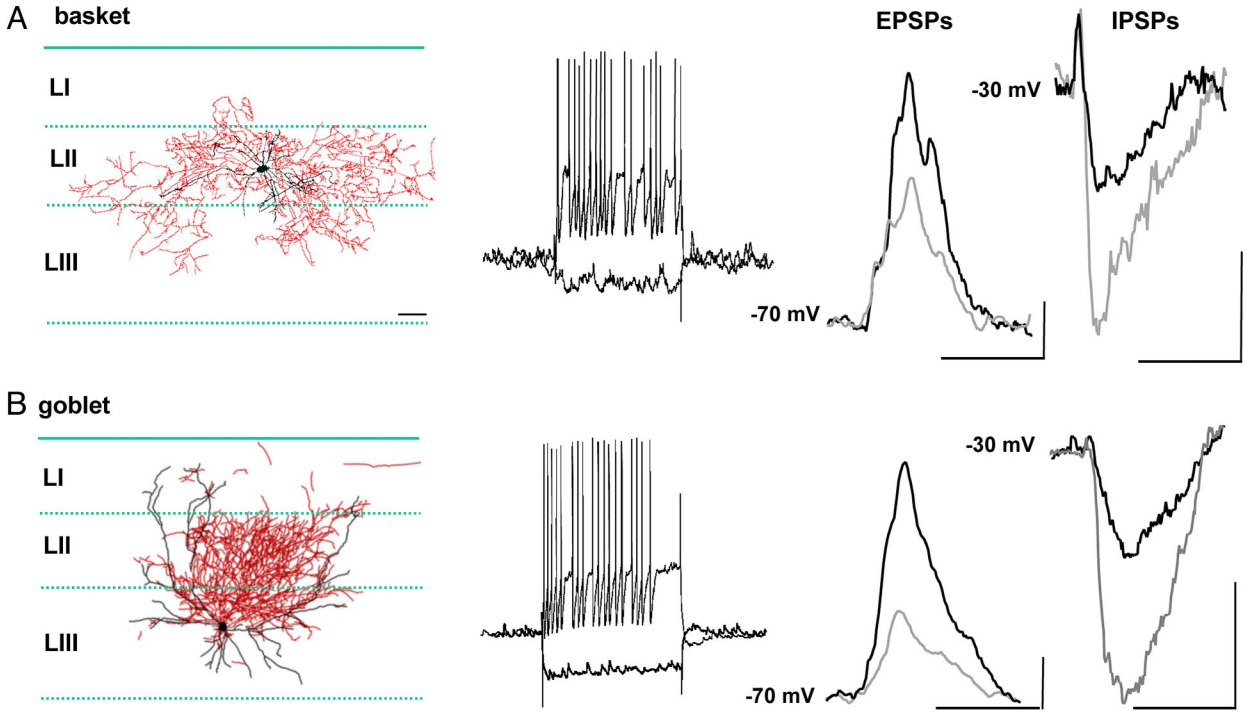

Fig. 2. Anatomical and electrophysiological characterization of basket and goblet interneurons in superficial mEC. (*A*) Neurolucida reconstruction of a basket interneuron showing predominant dendritic (black) and axonal (red) arborisation in LII. Step current injection, during control gamma rhythms from −70 mV, shows fast spiking behavior (+0.2 nA) and absence of overt sag and rebound (−0.1 nA). Basket interneurons showed large, compound excitatory postsynaptic potentials (EPSPs) on each gamma period. Data traces are average of 50 EPSPs averaged relative to peak depolarization. Note temporal separation of components of the compound EPSP is still evident after averaging (e.g., see ref. 6). Ketamine (black) increased mean EPSP amplitude compared with control conditions (gray). Baskets also displayed small amplitude inhibitory postsynaptic potentials (IPSPs) when depolarized to −30 mV. Ketamine (black) was associated with a reduction in mean interneuron IPSP amplitude from control (gray). Traces shown are average of 50 IPSPs. [Scale bars, 3 mV, 10 ms (EPSPs); 1 mV, 10 ms (IPSPs).] (*B*) Neurolucida reconstruction of a goblet interneuron showing dendritic and axonal arborisation in LII/III. Step current injection, during control gamma rhythms from a potential of −70 mV, showed fast spiking behavior (+0.2 nA) and small sag and rebound (−0.1 nA). Goblet interneurons also showed large amplitude, compound excitatory postsynaptic potentials (EPSPs) on each gamma period. Ketamine (black) increased mean EPSP amplitude compared with mean EPSP amplitude in control conditions (gray). Goblets, in contrast to baskets, displayed large amplitude IPSPs when depolarized to −30 mV. Ketamine (black) reduced mean goblet IPSP amplitude from control values (gray). Traces shown are average of 50 IPSPs. Scale bar for reconstructions, 100 μm. [Scale bars, 1 mV, 10 ms (EPSPs); 4 mV, 10 ms (IPSPs).] Note difference in scale bars for basket and goblet interneuron synaptic events.

potential maximum to AHP maximum was also significantly longer in goblet cells (2.7 ± 1.1 ms) than in basket cells (2.1 ± 2.2 ms) ($P < 0.05$, $n = 5$).

To better understand their relative roles in the two types of population rhythm recorded, we quantified excitatory and inhibitory synaptic inputs during control gamma oscillations and in the presence of ketamine. During control gamma rhythms, basket cells showed synaptic events dominated by phasic excitation. The mean amplitude of the compound EPSPs seen at −70 mV membrane potential was 7.2 ± 1.4 mV, whereas mean IPSP amplitude at −30 mV membrane potential was 2.0 ± 0.6 mV (Fig. 1*A*). The opposite relationship between inhibition and excitation was seen in goblet cells, with synaptic inputs dominated by inhibition. The mean amplitude of the compound EPSPs seen at −70 mV membrane potential was 1.8 ± 0.4 mV, whereas mean IPSP amplitude at −30 mV membrane potential was 8.2 ± 1.6 mV (Fig. 1*B*). Despite the contrasting strengths of synaptic excitation and inhibition in the two interneuron subtypes during control gamma rhythms, the application of ketamine, and switch to the lower power, slower field potential rhythm, produced similar effects in both cells. Mean compound EPSP amplitudes in both interneurons increased approximately twofold to 13.1 ± 2.5 mV (baskets, $n = 5$, $P < 0.05$) and 5.0 ± 1.3 mV (goblets, $n = 6$, $P < 0.05$). Mean IPSP amplitudes in both interneurons significantly decreased to 1.0 ± 0.3 mV (baskets, $n = 5$, $P < 0.05$) and 3.5 ± 0.8 mV (goblets, $n = 6$, $P < 0.05$). The kinetics of synaptic events in the two cell types were approximately the same. Mean halfwidth of compound EPSP onto both types of interneurons was not significantly different (basket: goblet, 6.3 ± 1.1 *v.* 7.8 ± 1.5 ms; $n = 5$, $P > 0.05$). There was also no significant difference between either interneuron cell type for rise time of the initial component of the compound EPSP (2.1 ± 0.2 v. 2.0 ± 0.3 ms). IPSP properties were also broadly similar with the mean halfwidths of IPSPs being basket: 9.1 ± 1.2, goblet: 10.8 ± 0.9 ms ($n = 5$, $P > 0.05$), and average rise time of IPSPs being 2.0 ± 0.2 (basket), 2.4 ± 0.2 mV (goblet).

A Superficial mEC Model with Two Different Interneuron Subtypes Accounts for the Experimental Observations. To understand whether the loss of NMDA receptor-mediated drive to basket cells alone was sufficient to reproduce the change in gamma power and frequency, the net increase in excitatory neuronal excitability, and the more subtle changes in synaptic inputs and spike rates in the two interneuron subtypes, we constructed a model of superficial mEC using the four neuronal subtypes recorded (Fig. 3*A*, see *SI Appendix*). This model was capable of reproducing the changes in population rhythms seen on ketamine application very accurately, with a change only in the degree of NMDA drive to basket cells (I-cells). Due to the alignment of the pyramidal cell dendrites, the field potential was hypothesized to be mainly due to synaptic currents onto the pyramidal cells (15). The power spectrum of the IPSPs onto the E cells matched the reduction in experimental gamma power under NMDA receptor block (Fig. 3*B*). In the control simulations, as in the experiment, individual pyramidal cells (E), stellate cells (S) and goblet interneurons (G) fired sparsely while the

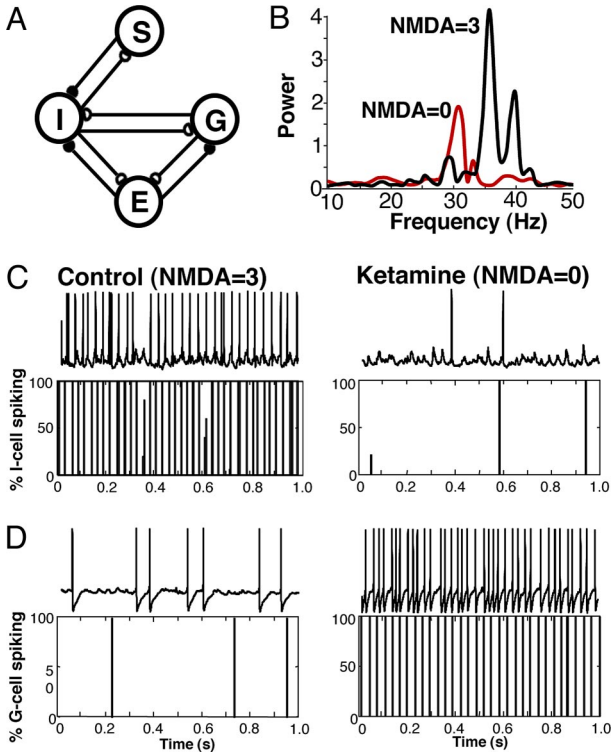

Fig. 3. A model superficial mEC circuit predicts differential involvement of the two interneuron subclasses. (*A*) Cartoon illustrating the basic model structure (see *Methods*) including: pyramidal cells (E), basket interneurons (I), goblet interneurons (G) and stellate cells (S). Both interneuron subtypes were connected to E-cells, S-cells and each other by fast inhibitory synapses (white symbols, see *SI Appendix*). Each interneuron subtype received fast excitatory synaptic input (black symbols) from both E-cells and S-cells. No recurrent excitatory connectivity between E-, and S-cells was included (47). (*B*) The model reproduces the main network dynamic changes seen on application of ketamine (cf. Fig. *1A*). Power spectra show ''population'' activity taken from the sum of all inhibitory synaptic inputs to the pyramidal cell population. Note the decrease in power and frequency on removal of the NMDA receptor-mediated drive to basket cells. (*C* and *D*) Relative spike rates in the two interneuron subtypes (basket, I-cell and Goblet, G-cell) show a switch in dominance in the circuit when NMDA drive to basket (I) cells was removed. One second traces of intracellular recordings from the two interneuron types are shown above corresponding spike time histograms from the model.

basket interneuron (I) population fired at a gamma frequency (41 Hz, Fig. 3 *C* and *D*). Their average individual cell frequency over 50 trials was 5.3 ± 1.5 Hz (E cells), 2.8 ± 0.6 Hz (S cells), 3 Hz (goblet cells) and 41.0 ± 0.6 Hz (basket cells).

The gamma rhythm (in both regimes) was formed by a PING (Pyramidal Interneuron Network Gamma) rhythm (20, 21) in which cycle by cycle white noise and the AHP current in the pyramids play an important role. A sufficiently large cluster of pyramids fire near synchronously and cause the interneuron population to fire near synchronously. The subsequent interneuron inhibition onto the pyramids serves to organize clusters that fire near synchronously to repeat the process. The bursts of theta rhythm in the goblet cell population required two factors: the strength of the synapse from basket to goblet cells had to be sufficiently strong to prevent the goblet cells from joining in the gamma rhythm (I-G synaptic conductance twice as strong as G-I), and the relatively strong h-current (almost as strong as in S cells) enabled them to escape from the strong gamma frequency IPSPs. The relative quiescence of the S cells resulted from the gamma frequency IPSPs received from the basket cells.

Removal of NMDA drive only to model basket cells switched the population rhythm from one dominated by the E/basket subnetwork to one formed by the E/goblet subnetwork. The gamma rhythm frequency was reduced to 32 Hz (Fig. 3*B*), and average individual E cell frequency over 50 trials increased to 9.8 ± 1.7 Hz; S-cell frequency also increased to 9.8 ± 0.4 Hz (Fig. S2), and average individual goblet cell frequency over 50 trials increased to 32 Hz (Fig. 3*D*). Consistent with experimental findings (Fig. 3*C*), the reduction in tonic drive to basket cells greatly reduced their firing (average individual basket cell frequency over 50 trials fell to 4.3 ± 3.5 Hz). This near decimation of basket cell firing frequency effectively released the goblet cells from gamma frequency inhibition and enabled a gamma rhythm to be produced between the E and goblet cells. A relatively weak goblet cell to E synaptic conductance, compared to basket to E conductance (factor of 3), was needed to reproduce the experimental reduction in gamma power under NMDA receptor block (Figs, 1*A*, 3*B*).

Relation to Intrinsic Gamma Rhythms in the Hippocampus Proper. During persistent gamma rhythms in intact hippocampal slices, the gamma rhythm is seen to be generated in area CA3 with frequencies between 30–40 Hz (2, 22), a generally lower frequency than that seen in control conditions in comparable mEC slice preparations (15, 17) (see above). However, multiple pathways for information transfer from mEC to the hippocampus proper exist (23), with direct and indirect inputs to CA1 converging on individual CA1 neurons (24). To test whether local circuits in area CA1 are more predisposed, when compared to those in area CA3, to forming temporal interactions through frequency matching with *direct* mEC gamma frequency input we exposed minislices of isolated CA1 and CA3 subfields to low concentrations of kainate (0.3–2.5 μM). Bath application of kainate to CA3 minislice (Fig. 4*A*) produced an oscillation with a peak frequency of 34 ± 3 Hz. This frequency was not significantly different from the slow gamma rhythm generated in mEC with NMDA receptors blocked (Fig. 4*B*, $P > 0.05$, $n = 4$) but was significantly different from the control mEC gamma rhythm ($P < 0.05$, $n = 4$). In contrast, in CA1 minislice (taken from the same full hippocampal slices used to prepare the CA3 minislices) kainate—at concentrations above 1 μM only—produced a significantly faster gamma rhythm with frequency 46 ± 4 Hz ($P < 0.05$ vs. CA3, $n = 4$) which better matched the control mEC gamma rhythm frequency when NMDA receptors were not blocked (Fig. 4*B*, $P > 0.05$ CA1 vs. mEC + ketamine, $n = 4$).

Discussion

NMDA receptor activation has long been associated with memory-related processes in the central nervous system (25, 26). The present data indicate that active NMDA receptors in mEC provide a tonic excitation predominantly to basket-like interneurons that facilitates the local generation of a high power, around 40 Hz, gamma rhythm produced by reciprocal phasic interaction between principal cells and basket cells. This roughly 40 Hz gamma rhythm was manifest as large amplitude phasic GABAergic inhibition in principal neuronal somata. In contrast, the absence of NMDA receptor-mediated excitation in mEC almost abolishes basket interneuron spiking, reducing the predominant synaptic inhibition of a second, novel subtype of interneuron (fast-spiking goblet-cells), thus allowing them to actively participate in the local, reciprocal principal cell-interneuron circuit. This goblet cell-mediated gamma rhythm was of lower frequency, around 30 Hz, but was associated with a much stronger output from principal cells.

The present study provides a mechanism by which two spectrally distinct frequencies of gamma rhythm can be generated in the same entorhinal area. The mathematical model of a simple superficial mEC circuit predicted that three key features were essential to produce the pattern of output differences seen for each gamma rhythm. Firstly, the "dominant" inhibitory neuron must have a component of excitation strongly dependent on NMDA receptor activation. LII basket cells in mEC fit this description (16). Secondly, the non-NMDA receptor-driven interneurons must have a

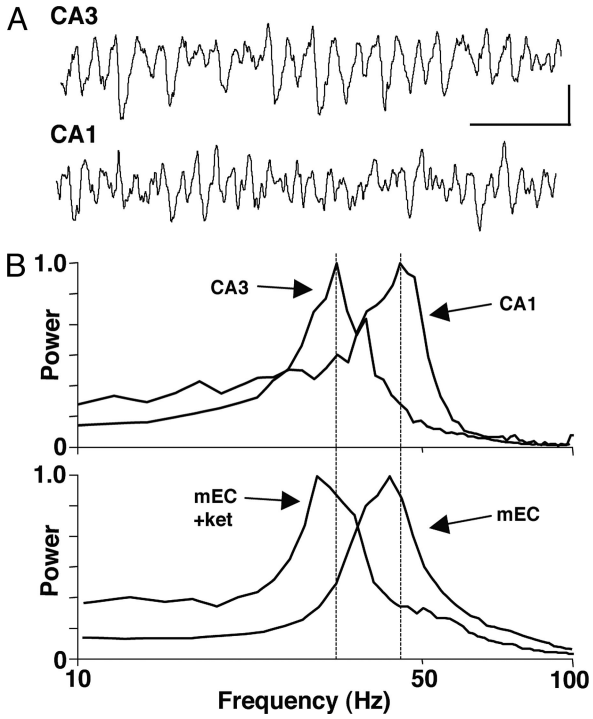

Fig. 4. The two mEC gamma rhythm frequencies, with and without active NMDA receptors, compare with intrinsic gamma frequencies in isolated CA3 and CA1 hippocampal networks. (*A*) Example local field potential recordings from stratum radiatum in slices of surgically isolated area CA3 and area CA1 in the presence of kainate. Note the larger, slower gamma rhythm generated by CA3 in isolation (cf. CA1). (Scale bars, 0.1 mV, 100 ms.) (*B*) Power spectra (n = 4) for 60 s epochs of population gamma activity in isolated CA3 and CA1 minislices. Data were normalized to peak power to illustrate the difference in modal peak frequency between the two areas. Lower graph shows pooled power spectra (n = 7) for population gamma rhythms in superficial layers of mEC in the presence (mEC + ket) and absence (mEC) of ketamine. Note the absence of NMDA receptor activity changes mEC frequency so that modal frequency changes from values similar to CA1 network activity, down to values similar to CA3 network activity.

strong inhibitory synaptic input, allowing them to be dominated by activity in the basket cells and also to generate a slower network rhythm—interneuronal GABAergic input amplitude having a major influence on network gamma frequency (7). A scenario that was clearly the case for goblet cells (see Fig. 4) and one that is unusual in gamma-generating interneurons as inhibitory synaptic input is often considerably weaker than excitatory synaptic input (27, 28). Finally, inhibitory synaptic output from goblet cells must be weaker than for basket cells. Such a difference was required to (*i*) produce the large increase in principal cell firing seen when changing from a basket interneuron-dominated to a goblet interneuron-dominated rhythm (e.g., Fig. S2) and (*ii*) produce the dramatic decrease in the power of the gamma rhythm observed in the presence of ketamine (e.g., Fig. 1*A* and 3*B*).

It is not yet clear why single regions of mEC can generate two different fundamental frequencies of gamma rhythm. However, it is interesting to note that the two frequencies seen correspond to the two frequencies generated by intrinsic network activity in areas CA1 and CA3 of the hippocampus. The higher gamma frequency more closely matches that of CA1 gamma band (29) and the lower gamma frequency that of area CA3. From a dynamical perspective, this matching of the two gamma frequencies in the entorhinal cortex with those in either CA3 or CA1 would be expected to have implications for hippocampal processing of signals from this region. When a phasic input (driver) to an oscillator (target) has approximately the same frequency as that oscillator, the two can phase-lock, creating coherence at which the relative phases of the input and output stay constant (30). Thus, the higher frequency, NMDA receptor-dependent gamma rhythm in mEC can "drive" that of CA1, and the slower, NMDA receptor-independent gamma rhythm can drive that of the CA3. If the frequencies are too different, it takes a much larger drive to lock phasic inputs to the target region's intrinsic frequency, if at all; in the absence of locking, the relative phases of the driver and target change cycle by cycle, implying that the effects of the driver on the target are also not reproducible cycle by cycle. It should be noted that the effects of a periodic drive on a network are more subtle than on a fixed oscillator (31); however, the closeness in frequency of the driver and target is still expected to be relevant to the efficacy and control of the driving. Interestingly, combining two different gamma frequencies with values around 30 Hz (from area CA3) and 40 Hz (directly from mEC)—as would be expected at the level of area CA1—produces a pattern of frequency beating within the hippocampal theta range (7–13 Hz), a mode of frequency interaction proposed, for theta frequencies, to underlie phase precession in hippocampus (32).

Interactions between the entorhinal cortex and hippocampus are associated with mnemonic processing in the brain (33, 34). In animal models and in humans, the dynamics of population activity in the two structures corresponds to performance in a number of cognitive tests involving memory (35, 36). Both structures are active during memory formation in humans (37), and phase synchrony between the two areas is seen during word learning tasks (38). However, this phase synchrony was seen over a broad range of frequencies (30–50 Hz) and evidence exists to suggest multiple gamma frequency generators at different anatomical locations along the hippocampal–entorhinal axis. It is therefore not clear which neuron subtypes and subregions are involved. For example, removal of entorhinal cortex in vivo produces a slower gamma rhythm (39), whose origins appear to be in area CA3 (40). Disruption of only the perforant path connection via dentate gyrus, however, preserves a faster gamma rhythm in area CA1 which is dependent on entorhinal drive (4). Thus it is possible that the two main pathways for information flow between entorhinal cortex and hippocampus (the trisynaptic pathway involving predominantly stellate cell outputs to dentate gyrus before activation of CA3, then CA1, and the monosynaptic, direct pathway involving pyramidal cell inputs to area CA1) may utilize different frequencies to temporally code activity patterns (41). These frequency-dependent pathways may, in turn, be selected by mEC on the basis of the temporal pattern of neocortical input. It has been shown previously that input frequency preference exists in mEC even down at single cell level (42).

The proposed two modes of entorhinal-hippocampal communication (above) may represent different cognitively relevant processes. For example, precise spatial firing in hippocampal place cells has been shown to require both the monosynaptic pathway and the trisynaptic pathway (43). However, pattern separation in hippocampus appears to correspond with activity along the CA3-DG part of the trisynaptic circuit whereas pattern completion occurs in area CA1 (44). In addition, differences in how the brain uses these two pathways for contextual learning have been seen. Fast, one-trial contextual learning is critically dependent on the trisynaptic circuit but the direct mEC-CA1 pathway is sufficient for slower, multitrial learning (45). The activation pattern of NMDA receptors in mEC may therefore be a factor in governing the proportion of each pathway used to process novel sensory information. It is interesting to note that change in NMDA receptor activation of mEC interneurons is a feature of acute and genetic models of schizophrenia-like psychosis (17). In these models, and in schizophrenia its self, disrupted entorhinal cortex function is linked to sensorimotor gating deficits (46), and general cognitive deficits involving some of the processes discussed here are apparent (47). Thus, it is possible that disruption of a single facet of synaptic communication (NMDA

receptors) may underlie macroscopic changes in the routing of information flow along this critical axis.

In summary, the strength and frequency of neuronal population outputs from mEC is controlled by the degree of NMDA receptor activation. Two interacting local circuits exist utilizing two different interneuron subtypes to generate two different gamma frequencies, temporally controlling the flow of information through two pathways around the hippocampus. The meeting point of these two pathways, and the frequency differences in the population input, suggest that context and content-specific information may be combined at the level of area CA1 via interactions between these two frequencies within the timeframe of hippocampal theta rhythm.

Methods

Experimental. Transverse medial entorhinal cortical (mEC) slices (450 μm) were prepared from adult Wistar rats and maintained according to methods used in ref. 16. Effects of NMDA receptor blockade were enhanced in the present study by reducing $[Mg^{2+}]_o$ from 2.0 to 1.2 mM. Full details of electrophysiological methods used are in the *SI Appendix*.

Modeling. To investigate the mechanisms for the experimentally observed rhythmic activity patterns, we modeled a local region of the superficial layers of the entorhinal cortex with a network consisting of a population of 100 pyramidal cells (E), a population of 10 basket cell interneurons (I), a population of 10 goblet interneurons (G), and a population of 20 stellate cells (S), (Fig. 3*A*, ref. 48, 49) Each neuron was modeled as a single compartment using biophysically-based Hodgkin-Huxley type equations, with full details of neuronal conductances and connectivity presented in the *SI Appendix*.

ACKNOWLEDGMENTS. We thank Dr C. Rind for help with neuronal reconstructions. We would also like to thank Jozsef Csicsvari and James Chrobak for their close reading and comments on this manuscript. This work was supported by the MRC (U.K.), The Royal Society, a YSU research professorship (J.J.), NSF/NIH CRCNS and The Wellcome Trust.

1. Vidal JR, Chaumon M, O'Regan JK, Tallon-Baudry C (2006) Visual grouping and the focusing of attention induce gamma-band oscillations at different frequencies in human magnetoencephalogram signals. *J Cogn Neurosci* 18:1850–1862.
2. Fisahn A, Pike FG, Buhl EH, Paulsen O (1998) Cholinergic induction of network oscillations at 40 Hz in the hippocampus *in vitro*. *Nature* 394:186–189.
3. Chrobak JJ, Buzsaki G (1998) Gamma oscillations in the entorhinal cortex of the freely behaving rat. *J Neurosci* 18:388–398.
4. Charpak S, Pare D, Llinas R (1995) The entorhinal cortex entrains fast CA1 hippocampal oscillations in the anaesthetized guinea-pig: Role of the monosynaptic component of the perforant path. *Eur J Neurosci* 7:1548–1557.
5. Whittington MA, Traub RD, Jefferys JG (1995) Synchronized oscillations in interneuron networks driven by metabotropic glutamate receptor activation. *Nature* 373:612–615.
6. Cunningham MO, *et al.* (2004) A role for fast rhythmic bursting neurons in cortical gamma oscillations *in vitro*. *Proc Natl Acad Sci USA* 101:7152–7157.
7. Faulkner HJ, Traub RD, Whittington MA (1998) Disruption of synchronous gamma oscillations in the rat hippocampal slice: A common mechanism of anaesthetic drug action. *Br J Pharmacol* 125:483–492.
8. Traub RD, Whittington MA, Colling SB, Buzsáki G, Jefferys JG (1996) Analysis of gamma rhythms in the rat hippocampus *in vitro* and *in vivo*. *J Physiol* 493:471–484.
9. Canolty RT, *et al.* (2006) High gamma power is phase-locked to theta oscillations in human neocortex. *Science* 313:1626–1628.
10. Hájos N, *et al.* (2004) Spike timing of distinct types of GABAergic interneuron during hippocampal gamma oscillations *in vitro*. *J Neurosci* 24:9127–37.
11. Tukker JJ, Fuentealba P, Hartwick K, Somogyi P, Klausberger T (2007) Cell type-specific tuning of hippocampal interneuron firing during gamma oscillations *in vivo*. *J Neurosci* 27:8184–8189.
12. Gloveli T, *et al.* (2005) Differential involvement of oriens/pyramidale interneurones in hippocampal network oscillations *in vitro*. *J Physiol* 562:131–147.
13. Whittington MA, Traub RD (2003) Interneuron diversity series: Inhibitory interneurons and network oscillations *in vitro*. *Trends Neurosci* 26:676–682.
14. Pálhalmi J, Paulsen O, Freund TF, Hájos N (2004) Distinct properties of carbachol- and DHPG-induced network oscillations in hippocampal slices. *Neuropharmacology* 47:381–389.
15. Cunningham MO, Davies CH, Buhl EH, Kopell N, Whittington MA (2003) Gamma oscillations induced by kainate receptor activation in the entorhinal cortex *in vitro*. *J Neurosci* 23:9761–9769.
16. Jones RS, Buhl EH (1993) Basket-like interneurones in layer II of the entorhinal cortex exhibit a powerful NMDA-mediated synaptic excitation. *Neurosci Lett* 149:35–39.
17. Cunningham MO, *et al.* (2006) Region-specific reduction in entorhinal gamma oscillations and parvalbumin-immunoreactive neurons in animal models of psychiatric illness. *J Neurosci* 26:2767–2776.
18. Herron CE, Lester RA, Coan EJ, Collingridge GL (1986) Frequency-dependent involvement of NMDA receptors in the hippocampus: A novel synaptic mechanism. *Nature* 322:265–268.
19. Chrobak JJ, Hinman JR, Sabolek HR (2008) Revealing past memories; proactive interference and ketamine-induced memory deficits. *J Neurosci* 28:4512–4530.
20. Whittington MA, Traub RD, Kopell N, Ermentrout B, Buhl EH (2000) Inhibition-based rhythms: Experimental and mathematical observations on network dynamics. *Int J Psychophysiol* 38:315–336.
21. Borgers C, Kopell N (2005) Effects of noisy drive on rhythms in networks of excitatory and inhibitory neurons. *Neural Comput* 17:557–608.
22. Hormuzdi SG, *et al.* (2001) Impaired electrical signaling disrupts gamma frequency oscillations in connexin 36-deficient mice. *Neuron* 31:487–495.
23. Witter MP (1993) Organization of the entorhinal-hippocampal system: A review of current anatomical data. *Hippocampus* 3:33–44.
24. Kajiwara R, *et al.* (2008) Convergence of entorhinal and CA3 inputs onto pyramidal neurons and interneurons in hippocampal CA1—and anatomical study in rat. *Hippocampus* 18:266–280.
25. Morris RG, Davis S, Butcher SP (1990) Hippocampal synaptic plasticity and NMDA receptors: A role in information storage? *Philos Trans R Soc Lond B* 329:187–204.
26. Morris RG (2006) Elements of a neurobiological theory of hippocampal function: The role of synaptic plasticity, synaptic tagging and schemas. *Eur J Neurosci* 23:2829–2846.
27. Traub RD, *et al.* (2000) A model of gamma-frequency network oscillations induced in the rat CA3 region by carbachol *in vitro*. *Eur J Neurosci* 12:4093–4106.
28. Oren I, Mann EO, Paulsen O, Hájos N (2006) Synaptic currents in anatomically identified CA3 neurons during hippocampal gamma oscillations *in vitro*. *J Neurosci* 26:9923–9934.
29. Bibbig A, *et al.* (2007) Beta rhythms (15–20 Hz) generated by non-reciprocal communication in hippocampus. *J Neurophysiol* 97:2812–2823.
30. Kopell N, Ermentrout GB (2002) Mechanisms of phase-locking and frequency control in pairs of coupled neural oscillators. *Handbook on Dynamical Systems*, volume 2: *Toward Applications*, ed Fiedler B (Elsevier, North Holland), pp 3–54.
31. Vierling-Claassen D, Seikmeyer P, Stufflebeam S, Kopell N (2008) Modeling GABA alterations in schizophrenia: A link between impaired inhibition and altered gamma and beta range inhibitory entrainment. *J Neurophysiol* 99:2656–2671.
32. O'Keefe J, Burgess N (2005) Dual phase and rate coding in hippocampal place cells: Theoretical significance and relationship to entorhinal grid cells. *Hippocampus* 15:853–866.
33. Segal M (1973) Dissecting a short-term memory circuit in the rat brain. I. Changes in entorhinal unit activity and responsiveness of hippocampal units in the process of classical conditioning. *Brain Res* 64:281–292.
34. Moss M, Mahut H, Zola-Morgan S (1981) Concurrent discrimination learning of monkeys after hippocampal, entorhinal, or fornix lesions. *J Neurosci* 1:227–240.
35. Chrobak JJ, Lörincz A, Buzsáki G (2000) Physiological patterns in the hippocampo-entorhinal cortex system. *Hippocampus* 10:457–465.
36. Fell J, Klaver P, Elger CE, Fernández G (2002) The interaction of rhinal cortex and hippocampus in human declarative memory formation. *Rev Neurosci* 13:299–312.
37. Fernández G, Brewer JN, Zhao Z, Glover GH, Gabrieli JD (1999) Level of sustained entorhinal activity at study correlates with subsequent cued-recall performance: A functional magnetic resonance imaging study with high acquisition rate. *Hippocampus* 9:35–44.
38. Fell J, *et al.* (2001) Human memory formation is accompanied by rhinal-hippocampal coupling and decoupling. *Nat Neurosci* 4:1159–1160.
39. Bragin A, *et al.* (1995) Gamma (40–100 Hz) oscillation in the hippocampus of the behaving rat. *J Neurosci* 15:47–60.
40. Csicsvari J, Jamieson B, Wise KD, Buzsáki G (2003) Mechanisms of gamma oscillations in the hippocampus of the behaving rat. *Neuron* 37:311–322.
41. Yeckel MF, Berger TW (1998) Spatial distribution of potentiated synapses in hippocampus: Dependence on cellular mechanisms and network properties. *J Neurosci* 18:438–450.
42. Alonso A, Klink R (1993) Differential electroresponsiveness of stellate and pyramidal-like cells of medial entorhinal cortex layer II. *J Neurophysiol* 70:128–143.
43. Brun VH, *et al.* (2008) Impaired spatial representation in CA1 after lesion of direct input from entorhinal cortex. *Neuron* 57:290–302.
44. Bakker A, Kirwan CB, Miller M, Stark CE (2008) Pattern separation in the human hippocampal CA3 and dentate gyrus. *Science* 319:1640–1642.
45. Nakashiba T, Young JZ, McHugh TJ, Buhl DL, Tonegawa S (2008) Transgenic inhibition of synaptic transmission reveals role of CA3 output in hippocampal learning. *Science* 319:1260–1264.
46. Goto K, Ueki A, Iso H, Morita Y (2002) Reduced prepulse inhibition in rats with entorhinal cortex lesions. *Behav Brain Res* 134:201–207.
47. Uhlhaas PJ, *et al.* (2006) Dysfunctional long-range coordination of neural activity during Gestalt perception in schizophrenia. *J Neurosci* 26:8168–8175.
48. Jalics J, Cunningham, MO, Kispersky TJ, Whittington MA, Kopell N (2006) Activation of different gamma-generating microcircuits in entorhinal cortex is NMDA receptor dependent. *Soc Neurosci Abs* 36:635.18.
49. Dhillon A, Jones RS (2000) Laminar differences in recurrent excitatory transmission in the rat entorhinal cortex *in vitro*. *Neuroscience* 99:413–422.